

Unsupervised Moving Object Detection via Contextual Information Separation

Yanchao Yang*
UCLA Vision Lab

yanchao.yang@cs.ucla.edu

Davide Scaramuzza
Robotics and Perception Group, ETH

sdavide@ifi.uzh.ch

Antonio Loquercio*
Robotics and Perception Group, ETH

loquercio@ifi.uzh.ch

Stefano Soatto
UCLA Vision Lab

soatto@cs.ucla.edu

Abstract

We propose an adversarial contextual model for detecting moving objects in images. A deep neural network is trained to predict the optical flow in a region using information from everywhere else but that region (context), while another network attempts to make such context as uninformative as possible. The result is a model where hypotheses naturally compete with no need for explicit regularization or hyper-parameter tuning. Although our method requires no supervision whatsoever, it outperforms several methods that are pre-trained on large annotated datasets. Our model can be thought of as a generalization of classical variational generative region-based segmentation, but in a way that avoids explicit regularization or solution of partial differential equations at run-time.

1. Introduction

Consider Fig. 1: Even relatively simple objects, when moving in the scene, cause complex discontinuous changes in the image. Being able to rapidly detect independently moving objects in a wide variety of scenes from images is functional to survival for animals and autonomous vehicles alike. We wish to endow artificial systems with similar capabilities, without the need to pre-condition or learn similar-looking backgrounds. This problem relates to motion segmentation, foreground/background separation, visual attention, video object segmentation as we discuss in Sect. 3. For now, we use the words “object” or “foreground” informally¹ to mean (possibly multiple) connected regions of the image domain, to be distinguished from their surrounding, which we call “background” or “context,” according to *some* cri-



Figure 1: An encounter between a hawk and a drone (top). The latter will not survive without being aware of the attack. Detecting moving objects is crucial to survival of animal and artificial systems alike. Note that the optical flow (middle row) is quite diverse within the region where the hawk projects: It changes both in space and time. Grouping this into a moving object (bottom row) is our goal in this work. Note the object is detected by our algorithm across multiple scales, partial occlusions from the viewpoint, and complex boundaries.

terion.

Since objects exist in the scene, not in the image, a method to infer them from the latter rests on an operational definition based on measurable image correlates. We call moving objects regions of the image whose motion cannot be explained by that of their surroundings. In other words, the motion of the background is uninformative of the motion of the foreground and vice-versa. The “information separation” can be quantified by the information reduction rate (IRR) between the two as defined in Sect. 2. This naturally translates into an adversarial inference criterion that has close connections with classical variational region-based segmentation, but with a twist: Instead of learning a generative model of a region that explains the image *in that region* as well as possible, our approach yields a model that tries to explain it *as poorly as possible* using measurements from *everywhere else but that region*.

*equal contribution

¹The precise meaning of these terms will be formalized in Sect. 2.

In generative model-based segmentation, one can always explain the image with a trivial model, the image itself. To avoid that, one has to impose model complexity bounds, bottlenecks or regularization. Our model does not have access to trivial solutions, as it is forced to predict a region without looking at it. What we learn instead is a contextual adversarial model, without the need for explicit regularization, where foreground and background hypotheses compete to explain the data with no pre-training nor (hyper)parameter selection. In this sense, our approach relates to adversarial learning and self-supervision as discussed in Sect. 3.

The result is a completely unsupervised method, unlike many recent approaches that are called unsupervised but still require supervised pre-training on massive labeled datasets and can perform poorly in contexts that are not well represented in the training set.

Despite the complete lack of supervision, our method performs competitively even compared with those that use supervised pre-training (Sect. 4).

Summary of Contributions

Our method captures the desirable features of variational region-based segmentation: Robustness, lack of thresholds or tunable parameters, no need for training. However, it does not require solving a partial differential equation (PDE) at run-time, nor to pick regularizers, or Lagrange multipliers, nor to restrict the model to one that is simple-enough to be tractable analytically. It also exploits the power of modern deep learning methods: It uses deep neural networks as the model class, optimizes it efficiently with stochastic gradient descent (SGD), and can be computed efficiently at run time. However, it requires no supervision whatsoever.

While our approach has close relations to both classical region-based variational segmentation and generative models, as well as modern deep learning-based self-supervision, discussed in detail in Sect. 3, to the best of our knowledge, it is the first *adversarial contextual model* to detect moving objects in images. It achieves better or similar performance compare to unsupervised methods on the three most common benchmarks, and it even edges out methods that rely on supervised pre-training, as described in Sect. 4. On one of the considered benchmarks, it outperforms all methods using supervision, which illustrates the generalizability of our approach. In Sect. 5 we describe typical failure modes and discuss limitations of our method. Our implementation will be open-sourced.

2. Method

We call “moving object(s)” or “foreground” any region of an image whose motion is unexplainable from the context. A “region of an image” Ω is a compact and multiply-

connected subset of the domain of the image, discretized into a lattice D . “Context” or “background” is the complement of the foreground in the image domain, $\Omega^c = D \setminus \Omega$. Given a measured image I and/or its optical flow to the next (or previous) image u , foreground and background are uncertain, and therefore treated as random variables. A random variable u_1 is “unexplainable” from (or “uninformed” by) another u_2 if their mutual information $\mathbb{I}(u_1; u_2)$ is zero, that is if their joint distribution equals the product of the marginals, $P(u_1, u_2) = P(u_1)P(u_2)$.

More specifically, the optical flow $u : D_1 \rightarrow D_2 \subset \mathbb{R}^2$ maps the domain of an image $I_1 : D_1 \rightarrow \mathbb{R}_+^3$ onto another D_2 of I_2 , so that if $x_i \in D_1$, then $x_i + u_i \in D_2$, where $u_i = u(x_i)$ up to a discretization into the lattice and cropping of the boundary. Ideally, if the brightness constancy constraint equation that defines optical flow was satisfied, we would have $I_1 \circ u = I_2$ point-wise.

If we consider the flow at two locations i, j , we can formalize the notion of foreground as a region Ω that is uninformed by the background:

$$\begin{cases} \mathbb{I}(u_i, u_j | I) > 0, i, j \in \Omega \\ \mathbb{I}(u_i, u_j | I) = 0, i \in \Omega, j \in D \setminus \Omega. \end{cases} \quad (1)$$

As one would expect, based on this definition, if the domain of an object is included in another, then they inform each other (see appendix).

2.1. Loss function

We now operationalize the definition of foreground into a criterion to infer it. We use the information reduction rate (IRR) γ , which takes two subsets $\mathbf{x}, \mathbf{y} \subset D$ as input and returns a positive scalar:

$$\gamma(\mathbf{x} | \mathbf{y}; I) = \frac{\mathbb{I}(u_{\mathbf{x}}, u_{\mathbf{y}} | I)}{\mathbb{H}(u_{\mathbf{x}} | I)} = 1 - \frac{\mathbb{H}(u_{\mathbf{x}} | u_{\mathbf{y}}, I)}{\mathbb{H}(u_{\mathbf{x}} | I)} \quad (2)$$

where \mathbb{H} denotes (Shannon) entropy. It is zero when the two variables are independent, but the normalization prevents the trivial solution (empty set).² As proven in the appendix, objects as we defined them are the regions that minimize the following loss function

$$\mathcal{L}(\Omega; I) = \gamma(\Omega | \Omega^c; I) + \gamma(\Omega^c | \Omega; I). \quad (3)$$

Note that \mathcal{L} *does not have a complexity term*, or regularizer, as one would expect in most region-based segmentation methods. This is a key strength of our approach, that involves no modeling hyperparameters, as we elaborate on in Sect. 3.

²A small constant $0 < \epsilon \ll 1$ is added to the denominator to avoid singularities, and whenever $\mathbf{x} \neq \emptyset$, $\mathbb{H}(u_{\mathbf{x}} | I) \gg \epsilon$, thus we will omit ϵ from now on.

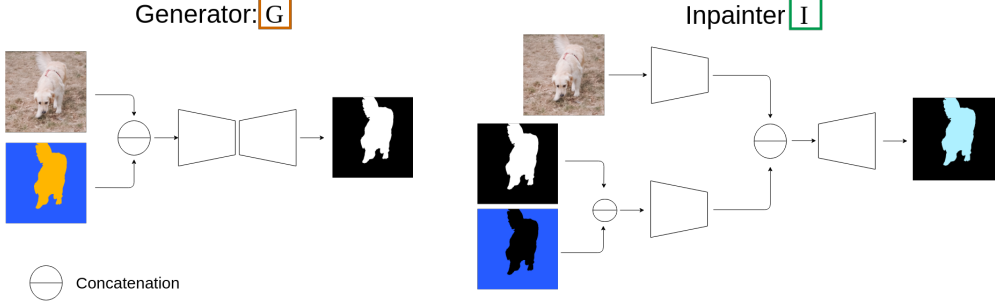


Figure 2: During training our method entails two modules. One is the generator (G), which produces a mask of the object by looking at the image and the associated optical flow. The other module is the inpainter (I), which tries to inpaint back the optical flow masked out by the corresponding mask. Both modules employ the encoder-decoder structure with skip connections, except that the inpainter (I) is equipped with two separate encoding branches. See section 4.1 for network details.

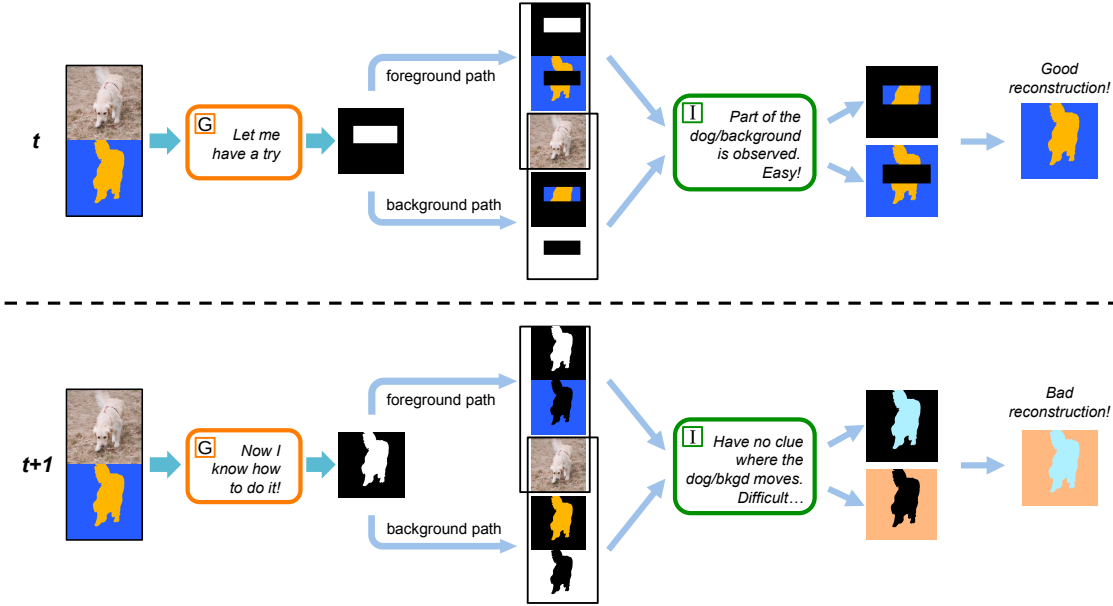


Figure 3: The two diagrams above show the learning process of the mask generator (G), when the inpainter (I) has already learned the conditionals to accurately inpaint the masked flow. The upper diagram shows that when the mask generated is not covering the object precisely, the inpainter will be informed about the optical flow in the mask by the flow in the context mask, and be able to make a good reconstruction. Similarly for the complement mask. However, in the lower diagram, when the object is precisely masked against the background, the inpainter (I) only observes the flow in the context, and has no information to predict the flow inside the object. Note that a randomly initialized inpainter (I) also knows nothing about the conditionals, thus we propose to jointly train both the generator (G) and the inpainter (I) in an adversarial manner as in Sect. 2.

Tame as it may look, (3) is intractable in general. For simplicity we indicate the flow inside the region(s) Ω (foreground) with $u^{\text{in}} = \{u_i, i \in \Omega\}$, and similarly for u^{out} , the flow in the background Ω^c . The only term that matters in the IRR is the ratio $\mathbb{H}(u^{\text{in}}|u^{\text{out}}, I)/\mathbb{H}(u^{\text{in}}|I)$, which is

$$\frac{\int \log P(u^{\text{in}}|u^{\text{out}}, I) dP(u^{\text{in}}, u^{\text{out}}|I)}{\int \log P(u^{\text{in}}|I) dP(u^{\text{in}}|I)} \quad (4)$$

that measures the information transfer from the background to the foreground. This is minimized when knowledge of the background flow is sufficient to predict the foreground.

To enable computation, we have to make draconian, yet common, assumptions on the underlying probability model, namely that

$$P(u^{\text{in}} = x|I) \propto \exp\left(-\frac{\|x\|^2}{\sigma^2}\right) \quad (5)$$

$$P(u^{\text{in}} = x|u^{\text{out}} = y, I) \propto \exp\left(-\frac{\|x - \phi(\Omega, y, I)\|^2}{\sigma^2}\right)$$

where $\phi(\Omega, y, I) = \int u^{\text{in}} dP(u^{\text{in}}|u^{\text{out}}, I)$ is the conditional mean given the image and the complementary observation.

Here we assume $\phi(\Omega, \emptyset, I) = 0$, since given a single image the most probable guess of the flow is zeros. With these assumptions, (4) can be simplified, to

$$\frac{\int \|u^{\text{in}} - \phi(\Omega, u^{\text{out}}, I)\|^2 dP(u^{\text{in}}, u^{\text{out}}|I)}{\int \|u^{\text{in}}\|^2 dP(u^{\text{in}}|I)} \approx \frac{\sum_{i,j=1}^N \|u_i - \phi(\Omega, u_j, I)\|^2}{\sum_{i=1}^N \|u_i\|^2} \quad (6)$$

where $N = |\mathcal{D}|$ is the cardinality of \mathcal{D} , or the number of flow samples available. Finally, our loss (3) to be minimized can be approximated as

$$\mathcal{L}(\Omega; I) = 1 - \frac{\sum_{i=1}^N \|u_i^{\text{in}} - \phi(\Omega, u_j^{\text{out}}, I)\|^2}{\sum_{i=1}^N \|u_i^{\text{in}}\|^2 + \epsilon} + 1 - \frac{\sum_{i=1}^N \|u_i^{\text{out}} - \phi(\Omega^c, u_j^{\text{in}}, I)\|^2}{\sum_{i=1}^N \|u_i^{\text{out}}\|^2 + \epsilon}. \quad (7)$$

In order to minimize this loss, we have to choose a representation for the unknown region Ω and for the function ϕ .

2.2. Function class

The region Ω that minimizes (7) belongs to the power set of D , that is the set of all possible subsets of the image domain, which has exponential complexity.³ We represent it with the indicator function

$$\begin{aligned} \chi : D &\rightarrow \{0, 1\} \\ i &\mapsto 1 \text{ if } i \in \Omega; 0 \text{ otherwise} \end{aligned} \quad (8)$$

so that the flow inside the region Ω can be written as $u_i^{\text{in}} = \chi u_i$, and outside as $u_i^{\text{out}} = (1 - \chi)u_i$.

Similarly, the function ϕ is non-linear, non-local, and high-dimensional, as it has to predict the flow in a region of the image of varying size and shape, given the flow in a different region. In other words, ϕ has to capture the context of a region to *recover* its flow.

Characteristically for the ages, we choose both ϕ and χ to be in the parametric function class of deep convolutional neural networks, as shown in Fig. 2, the specifics of which are in Sect. 4.1. We indicate the parameters with w , and the corresponding functions ϕ_{w_1} and χ_{w_2} . Accordingly, after discarding the constants, the *negative* loss (7) can be written as a function of the parameters

$$\begin{aligned} \mathcal{L}(w_1, w_2; I) = & \frac{\sum_{i \in D} |\chi_{w_2} u_i - \phi_{w_1}((1 - \chi_{w_2})u, I)_i|^2}{\sum_{i \in D} |\chi_{w_2} u_i|^2} + \\ & + \frac{\sum_{i \in D} |(1 - \chi_{w_2})u_i - \phi_{w_1}(\chi_{w_2} u, I)_i|^2}{\sum_{i \in D} |(1 - \chi_{w_2})u_i|^2}. \end{aligned} \quad (9)$$

³In the continuum, it belongs to the infinite-dimensional set of compact and multiply-connected regions of the unit square.

ϕ_{w_1} is called the *inpainter network*, and must be chosen to *minimize* the loss above. At the same time, the region Ω , represented by the parameters w_2 of its indicator function χ_{w_2} called *mask generator network*, should be chosen so that u^{out} is as uninformative as possible of u^{in} , and therefore the same loss is *maximized* with respect to w_2 . This naturally gives rise to a minimax problem:

$$\hat{w} = \arg \min_{w_1} \max_{w_2} \mathcal{L}(w_1, w_2; I). \quad (10)$$

This loss has interesting connections to classical region-based segmentation, but with a twist as we discuss next.

3. Relation to Prior Work

To understand the relation of our approach to classical methods, consider the simplest model for region-based segmentation [9]

$$L(\Omega, c_i, c_o) = \int_{\Omega} |u^{\text{in}}(x) - c_i|^2 dx + \int_{\Omega^c} |u^{\text{out}}(x) - c_o|^2 dx \quad (11)$$

typically combined with a regularizing term, for instance the length of the boundary of Ω . This is a convex infinite-dimensional optimization problem that can be solved by numerically integrating a partial differential equation (PDE). The result enjoys significant robustness to noise, provided the underlying scene has piecewise constant radiance and is measured by image irradiance, to which it is related by a simple “signal-plus-noise” model. Not many scenes of interest have piecewise constant radiance, although this method has enjoyed a long career in medical image analysis. If we enrich the model by replacing the constants c_i with smooth functions, $\phi_i(x)$, we obtain the celebrated Mumford-Shah functional [23], also optimized by integrating a PDE. Since smooth functions are an infinite-dimensional space, regularization is needed, which opens the Pandora box of regularization criteria, not to mention hyperparameters: Too much regularization and details are missed; too little and the model gets stuck in noise-induced minima. A modern version of this program would replace $\phi(x)$ with a parametrized model $\phi_w(x)$, for instance a deep neural network with weights w pre-trained on a dataset \mathcal{D} . In this case, the loss is a function of w , with natural model complexity bounds. Evaluating ϕ at a point inside, $x \in \Omega$, requires knowledge of the entire function u *inside* Ω , which we indicate with $\phi(x, u^{\text{in}})$:

$$\int_{\Omega} |u^{\text{in}}(x) - \phi_w(x, u^{\text{in}})|^2 dx + \int_{\Omega^c} |u^{\text{out}}(x) - \phi_w(x, u^{\text{out}})|^2 dx. \quad (12)$$

Here, a network can just map $\phi(x, u^{\text{in}}) = u^{\text{in}}$ providing a trivial solution, avoided by introducing (architectural or information) bottlenecks, akin to explicit regularizers. We

turn the table around and use the outside to predict the inside and vice-versa:

$$\int_{\Omega} |u^{\text{in}}(x) - \phi_w(x, u^{\text{out}})|^2 dx + \int_{\Omega^c} |u^{\text{out}}(x) - \phi_w(x, u^{\text{in}})|^2 dx \quad (13)$$

After normalization and discretization, this leads to our loss function (7). The two regions compete: for one to grow, the other has to shrink. In this sense, our approach relates to region competition methods, and specifically Motion Competition [13], but also to adversarial training, since we can think of ϕ as the generator (the inpainting network [4], that generates a flow inside) and then the “discriminator” present in a classification problem (GAN [1]) is replaced with a regressor, reflected in the loss function we use. This also relates to what is called “self-supervised learning,” a misnomer since there is no supervision, just a loss function that does not involve externally annotated data. Several variants of our approach can be constructed by using different norms, or correspondingly different models for the joint and marginal distributions (5).

More broadly, the ability to detect independently moving objects is primal, so there is a long history of motion-based segmentation, or moving object detection. Early attempts to explicitly model occlusions include the layer model [35] with piecewise affine regions, with computational complexity improvements using graph-based methods [27] and variational inference [12, 7, 29] to jointly optimize for motion estimation and segmentation; [24] use of long-term temporal consistency and color constancy, making however the optimization more difficult and sensitive to parameter choices. Similar ideas were applied to motion detection in crowds [6], traffic monitoring [5] and medical image analysis [14]. Our work also related to the literature on visual attention [16, 8].

More recent data-driven methods [33, 32, 10, 28] learn discriminative spatio-temporal features and differ mainly for the type of inputs and architectures. Inputs can be either image pairs [28, 10] or image plus dense optical flow [33, 32]. Architectures can be either time-independent [32], or with recurrent memory [33, 28]. Overall, those methods outperform traditional ones on benchmark datasets [24, 26], but at the cost of requiring a large amount of labeled training data and with evidence of poor generalization to previously unseen data. For example, compare [32] in Table 2 and 4.

It must be noted that, unlike in Machine Learning at large, it is customary in video object segmentation to call “*unsupervised*” methods that *do* rely on massive amounts of manually annotated data, so long as they do not require manual annotation at run-time. We adopt the broader use of the term where unsupervised means that there is no supervision of any kind both at training and test time.

Like classical variational methods, our approach does not need any annotated training data. However, like modern

learning methods, our approach learns a contextual model, which would be impossible to engineer given the complexity of image formation and scene dynamics.

4. Experiments

We compare our approach to a set of state-of-the-art baselines on the task of video object segmentation to check the accuracy of the detection. We first present experiments on a controlled toy-example where the assumptions of our model are perfectly satisfied. The aim of this experiment is to get a sense of the capabilities of the presented approach in ideal conditions. In the second set of experiments, we evaluate the effectiveness of the proposed model on three public, widely used datasets: Densely Annotated Video Segmentation (DAVIS) [26], Freiburg-Berkeley Motion Segmentation (FBMS59) [24], and SegTrackV2 [34], that differs significantly in terms of appearance and image quality from the DAVIS and FBMS datasets. While the DAVIS dataset has always a single object per scene, FBMS and SegTrackV2 scenes can contain multiple objects per frame. To test the potential of our approach, we compare its performance to state-of-the-art methods for video object segmentation. We show that our method not only outperforms the unsupervised approaches, but even edges out other supervised algorithms that, in contrast to ours, have access to a large amount of labeled data with precise manual segmentation at training time. For quantitative evaluation, we employ the most common metric for video object segmentation, *i.e.* the mean Jaccard score, a.k.a. intersection-over-union score, \mathcal{J} . Given space constraints, we add additional evaluation metrics in the appendix.

4.1. Implementation and Networks Details

Generator, G: Depicted on the left of Fig. 3, the generator architecture is a shrunk version of SegNet [2]. Its encoder part consists of 5 convolutional layers each followed by batch normalization, reducing the input image to $\frac{1}{4}$ of its original dimensions. The encoder is followed by a set of 4 atrous convolutions with increasing radius (2,4,8,16). The decoder part consists of 5 convolutional layers, that, with upsampling, generate an output with the same size of the input image. As in SegNet [2], a final softmax layer generates the probabilities for each pixel to be foreground or background. The generator input consists of an RGB image I_t and the optical flow $u_{t:t+\delta T}$ between I_t and $I_{t+\delta T}$. At training time, δT is randomly sampled from the uniform distribution $\mathcal{U} = [-5, 5]$, with $\delta T \neq 0$. The optical flow $u_{t:t+\delta T}$ is generated with the pretrained PWC network [30], given its state-of-the-art accuracy and efficiency. The generator network has a total of 3.4M parameters.

Inpainter, I: We adapt the architecture of CPN [37] to build our inpainter network. Its structure is depicted on the right of Fig. 3. The input to this network consists of the

	DAVIS [26]	FBMS59 [24]	SegTrackV2 [34]
$\mathcal{J} \uparrow$	92.5	88.5	92.1

Table 1: **Performance under ideal conditions:** When the assumptions made by our model are fully satisfied, our approach can successfully detect moving objects.. Indeed, our model reaches near maximum Jaccard score in all considered datasets.

input image I_t and the flow masked according to the generator output, $\chi \odot u$, the latter concatenated with χ . Differently from the CPN, these two branches are balanced, and have the same number of parameters. The encoded features are then concatenated and passed to the CPN decoder, that outputs an optical flow $\hat{u} = \phi(\chi u, \chi, I_t)$ of the same size of the input image. Our inpainter network has a total of 1.5M parameters.

At test time, only the generator G is used. Given I_t and $u_{t:t+\delta T}$, it outputs a probability for each pixel to be foreground or background, $P_t(\delta T)$. To encourage temporal consistency, we compute the temporal average:

$$\overline{P}_t = \sum_{\delta T=-5, \neq 0}^{\delta T=5} P_t(\delta T) \quad (14)$$

The final mask χ is generated with a CRF [20] post-processing step on the final \overline{P}_t . More details about the post-processing can be found in the appendix.

4.2. Experiments in Ideal Conditions

Our method relies on basic, fundamental assumptions: *The optical flow of the foreground and of the background are independent.* To get a sense of the capabilities of our approach in ideal conditions, we artificially produce datasets where this assumption is fully satisfied. The datasets are generated as a modification of DAVIS2016 [26], FMBS [24], and SegTrackV2 [34]. While images are kept unchanged, ground truth masks are used to artificially perturb the optical flow generated by PWC [30] such that foreground and background are statistically independent. More specifically, a different (constant) optical flow field is sampled from a uniform distribution independently at each frame, and associated to the foreground and the background, respectively. More details about the generation of those datasets can be found in the Appendix. As it is possible to observe in Table 1, our method reaches very high performance in all considered datasets. This confirms the validity of our algorithm and that our loss function (10) is a valid and tractable approximation of the functional (3).

4.3. Performance on Video Object Segmentation

As previously stated, we use the term *Unsupervised* with a different meaning with respect to its definition in literature of video object segmentation. In our definition, and for what follows, the supervision refers to the algorithm’s usage, at training time, of ground truth object annotations. In contrast, it is common in the literature to define as semi-supervised the methods that, at test time, assume that the ground-truth segmentation of the first frame is known [3, 22], which could be posed as tracking problem [38, 39] since the detection of the target is done by human. Here we focus on moving object detection, and thus we compare to the methods that are usually referred to as “unsupervised” in the video object segmentation domain. However we make further differentiation on whether the ground truth object segmentation is needed (supervised) or not (truly unsupervised) during training.

In this section we compare our method with other 8 methods that represent the state of the art for moving object segmentation. In table 2 we can observe the performance of our method on the DAVIS2016 dataset [26]. Our approach outperforms the majority of the considered baselines, including the ones that need a large amount of labelled data at training time, *i.e.* FSEG [17] and LMP [32].

Table 3 shows the performance of our method on FBMS59 [24]. In this dataset, we outperform all the unsupervised methods and have comparable performance to the supervised methods. Interestingly, the score of the best performing unsupervised method on DAVIS2016, ARP [19], drops significantly in this new benchmark, probably due to the method’s overfitting to the DAVIS2016 dataset. It is also interesting to notice that the supervised LMP [32] trained on DAVIS2016, drops to half its performance on FBMS59. This is one of the primary motivations for our approach, that can be finetuned on any data, without the need for the latter to be annotated.

In our final set of experiments, we evaluate our performance on the SegTrackV2 dataset [34]. This dataset is particularly challenging since it can contain multiple moving objects per frame. Also, some frames have very low resolution and are motion blurred. As it is possible to observe in Table 4, our method outperforms all the supervised methods in this dataset. Indeed, it appears that those methods, trained on completely different looking images, have difficulties with the covariate shift due to changes in the data distribution. In addition to the supervised methods, our method also outperforms almost all the unsupervised ones. The only exception is NLC [15], since it was specifically designed to address this dataset, but significantly drops in performance on other data (see Table 2).

	PDB [28]	LVO [33]	FSEG [17]	LMP [32]	ARP [19]	SFL [11]	FTS [25]	NLC [15]	Ours
$\mathcal{J} \uparrow$	77.2	75.9	70.7	70.0	76.2	67.4	55.8	55.1	71.5

Table 2: **Performance on DAVIS2016 [26]:** Methods in blue require ground truth annotations at training time, while the ones in red are unsupervised. Our approach reaches comparable performance to the state-of-the-art, outperforming several supervised methods.

	PDB [28]	FSEG [17]	LVO [33]	LMP [32]	SAGE [36]	ARP [19]	SFL [11]	FTS [25]	Ours
$\mathcal{J} \uparrow$	74.0	68.4	65.1	35.7	61.2	59.8	55.0	47.7	63.6

Table 3: **Performance on FBMS59 [24]:** The method color scheme is the same as in Table 2. Our method outperforms all unsupervised methods as well as the majority of supervised ones.

4.4. Qualitative experiments and Failure Cases

In Fig. 4 we show a qualitative comparison of the detection generated by ours and others’ methods on the DAVIS dataset. As it is possible to observe, our algorithm can segment precisely the moving object regardless of cluttered background, occlusions, or large depth discontinuities. The typical failure case of our method consists in the detection of objects whose motion is due to the primary object. An example is given in the last row of Fig. 4, where the water moved by the surfer is also classified as foreground by our algorithm.

4.5. Training and Runtime Analysis

The generator and inpainter network’s parameters are trained at the same time by minimizing the functional (10). The optimization time is approximately 6 hours on a single GPU Nvidia Titan XP 1080i. Since both our generator and inpainter networks are relatively small, we can afford very fast training/finetuning times. This is in contrast to larger modules, *e.g.* PDB [28], that require up to 40 hrs of training.

At test time, predictions \bar{P}_t (defined in eq. 14) are generated at 3.15 FPS, or with an average time of 320ms per frame, including the time to compute optical flow with PWC [30]. If excluding the time to generate optical flow, our model can generate predictions at 10.2 FPS, or 98ms per frame. All previous timing do not include the CRF post-processing step. The results are summarized in Table 5.

5. Discussion

We have introduced a contextual adversarial model for moving object detection, based on information separation between foreground and background. The foreground (object) can be multiply-connected. Our model shows some strengths, and has limitations.

The strengths relate to the ability of the model to learn complex relations between foreground and background, that

allows us to separate objects in ways that a generative model cannot, even when one plays with regularization parameters extensively. This is made possible by using modern deep neural network architectures, like SegNet [2] and CPN [37], but does not require pre-training on massive annotated datasets.

This can be seen as a strength but also a limitation: If massive datasets are available, why not use them? In part because even massive is not large enough: There is evidence that models pre-trained on all available datasets still suffer performance drops whenever a new benchmark appears that has a significant covariate shift, as we show in the experiments. Moreover, our method outperforms models that require pre-training, despite being in principle at a disadvantage compared to them.

Our method is illustrated on motion-based segmentation, where the starting point is optical flow. One could argue that optical flow is costly, local, error-prone, all valid concerns. Our approach is general, and could be applied to other statistics than optical flow. Such extensions are part of our future work agenda. However, we find that moving object segmentation is a blocker to many applications in autonomy and we therefore focus on this problem first.

Another possible limitation is that we do not make full use of the image: In some cases, the optical flow is ambiguous, in others intensity, but rarely is the combination of the two insufficient. Again, our framework allows in theory exploitation of both, and we intend to expand in this direction. Having said that, our method does make use of the image as a conditioning factor in the inpainter network.

Our definition of objects, and the resulting inference criterion, is related to generative model-based segmentation and region-based methods popular in the nineties, but with an important difference: Instead of using the evidence inside a region to infer a model of that region that is as accurate as possible, we use evidence *everywhere else but* that region to infer a model within, and we seek that model to be as bad as possible. This relation, explored in detail in

	FSEG [17]	PDB [28]	LVO [33]	NLC [15]	CUT [18]	FTS [25]	Ours
$\mathcal{J} \uparrow$	61.4	60.9	57.3	67.2	54.3	47.8	62.0

Table 4: **Performance on SegTrackV2 [34]:** Same color scheme of Table 2 applies here. Our method outperforms all the supervised methods and the majority of the unsupervised ones.



Figure 4: **Qualitative Results:** the above figure compares qualitative the performance of our approach with several state-of-the-art, compared with the Ground-Truth (GT). As it is possible to see, our prediction are robust to background clutter, large depth discontinuities, and occlusions. The last row shows a typical failure case of our method, *i.e.* the detection as foreground of objects moved by the primary objects (water is moved by the surfer in this case).

	w/ flow	w/o flow
FPS	3.2	10.2
T[s]	0.32	0.098

Table 5: **Run-time analysis:** Computation time for our method evaluated including optical flow computation (w flow) and excluding it (w/o flow).

Sect. 3, forces learning a contextual model of the image, which is not otherwise the outcome of a generative model in region-based segmentation. For instance, if we choose a rich enough model class, we can trivially model the appearance of an object inside an image region as the image itself.

This is not an option in our model: We can only predict the inside of a region by looking outside of it. This frees us from having to impose modeling assumptions to avoid trivial solutions, but requires a much richer class of function to harvest contextual information.

This naturally gives rise an adversarial (min-max) optimization: An inpainter network, tries to hallucinate the flow inside from the outside. Another network, a discriminator or regressor, tries to force the inpainting network to do the lousiest possible job.

Finally, our method is easy to test as it requires no annotation whatsoever. It is not a learning method proper, but uses deep networks as a powerful function class to learn contextual models based on an information criterion. The implementation will be open-sourced.

References

- [1] M. Arjovsky, S. Chintala, and L. Bottou. Wasserstein gan. *arXiv preprint arXiv:1701.07875*, 2017. 5
- [2] V. Badrinarayanan, A. Kendall, and R. Cipolla. SegNet: A deep convolutional encoder-decoder architecture for image segmentation. *IEEE Transactions on Pattern Analysis and Machine Intelligence (PAMI)*, 39(12):2481–2495, 2017. 5, 7
- [3] L. Bao, B. Wu, and W. Liu. Cnn in mrf: Video object segmentation via inference in a cnn-based higher-order spatio-temporal mrf. In *IEEE Conference on Computer Vision and Pattern Recognition (CVPR)*. 6
- [4] M. Bertalmio, G. Sapiro, V. Caselles, and C. Ballester. Image inpainting. In *Proceedings of the 27th annual conference on Computer graphics and interactive techniques*, pages 417–424. ACM Press/Addison-Wesley Publishing Co., 2000. 5
- [5] D. Beymer, P. McLauchlan, B. Coifman, and J. Malik. A real-time computer vision system for measuring traffic parameters. In *IEEE Conference on Computer Vision and Pattern Recognition (CVPR)*, 1997. 5
- [6] G. Brostow and R. Cipolla. Unsupervised bayesian detection of independent motion in crowds. In *IEEE Conference on Computer Vision and Pattern Recognition (CVPR)*. IEEE, 2006. 5
- [7] T. Brox, A. Bruhn, and J. Weickert. Variational motion segmentation with level sets. In *IEEE European Conference on Computer Vision (ECCV)*, pages 471–483. 2006. 5
- [8] Z. Bylinskii, E. M. DeGennaro, R. Rajalingham, H. Ruda, J. Zhang, and J. K. Tsotsos. Towards the quantitative evaluation of visual attention models. *Vision research*, 116:258–268, 2015. 5
- [9] T. F. Chan and L. A. Vese. Active contours without edges. *IEEE TRANSACTIONS ON IMAGE PROCESSING*, 10(2), 2001. 4
- [10] J. Cheng, Y.-H. Tsai, S. Wang, and M.-H. Yang. SegFlow: Joint learning for video object segmentation and optical flow. In *IEEE International Conference on Computer Vision (ICCV)*, 2017. 5
- [11] J. Cheng, Y.-H. Tsai, S. Wang, and M.-H. Yang. SegFlow: Joint learning for video object segmentation and optical flow. In *IEEE International Conference on Computer Vision (ICCV)*, 2017. 7, 8
- [12] D. Cremers and S. Soatto. Motion competition: A variational approach to piecewise parametric motion segmentation. *IEEE International Journal of Computer Vision*, 62(3):249–265, 2004. 5
- [13] D. Cremers and S. Soatto. Motion competition: A variational approach to piecewise parametric motion segmentation. *International Journal of Computer Vision*, 62(3):249–265, 2005. 5
- [14] A. Elnakib, G. Gimelfarb, J. S. Suri, and A. El-Baz. Medical image segmentation: a brief survey. In *Multi Modality State-of-the-Art Medical Image Segmentation and Registration Methodologies*, pages 1–39. Springer, 2011. 5
- [15] A. Faktor and M. Irani. Video object segmentation by non-local consensus voting. In *British Machine Vision Conference (BMVC)*. British Machine Vision Association, 2014. 6, 7, 8
- [16] L. Itti and C. Koch. A saliency-based search mechanism for overt and covert shifts of visual attention. *Vision research*, 40(10-12):1489–1506, 2000. 5
- [17] S. D. Jain, B. Xiong, and K. Grauman. FusionSeg: Learning to combine motion and appearance for fully automatic segmentation of generic objects in videos. In *IEEE Conference on Computer Vision and Pattern Recognition (CVPR)*, 2017. 6, 7, 8
- [18] M. Keuper, B. Andres, and T. Brox. Motion trajectory segmentation via minimum cost multicuts. In *IEEE International Conference on Computer Vision (ICCV)*, 2015. 8
- [19] Y. J. Koh and C.-S. Kim. Primary object segmentation in videos based on region augmentation and reduction. In *IEEE Conference on Computer Vision and Pattern Recognition (CVPR)*, 2017. 6, 7
- [20] P. Krähenbühl and V. Koltun. Efficient inference in fully connected crfs with gaussian edge potentials. In *Advances in neural information processing systems*, pages 109–117, 2011. 6
- [21] D. Lao and G. Sundaramoorthi. Extending layered models to 3d motion. In *IEEE European Conference on Computer Vision (ECCV)*, 2018. 8
- [22] K.-K. Maninis, S. Caelles, Y. Chen, J. Pont-Tuset, L. Leal-Taixé, D. Cremers, and L. Van Gool. Video object segmentation without temporal information. *IEEE Transactions on Pattern Analysis and Machine Intelligence (TPAMI)*, 2018. 6
- [23] D. Mumford and J. Shah. Optimal approximations by piecewise smooth functions and associated variational problems. *Communications on pure and applied mathematics*, 42(5):577–685, 1989. 4
- [24] P. Ochs, J. Malik, and T. Brox. Segmentation of moving objects by long term video analysis. *IEEE Transactions on Pattern Analysis and Machine Intelligence (PAMI)*, 36(6):1187–1200, 2014. 5, 6, 7
- [25] A. Papazoglou and V. Ferrari. Fast object segmentation in unconstrained video. In *IEEE International Conference on Computer Vision (ICCV)*, 2013. 7, 8
- [26] F. Perazzi, J. Pont-Tuset, B. McWilliams, L. V. Gool, M. Gross, and A. Sorkine-Hornung. A benchmark dataset and evaluation methodology for video object segmentation. In *IEEE Conference on Computer Vision and Pattern Recognition (CVPR)*, 2016. 5, 6, 7
- [27] J. Shi and J. Malik. Motion segmentation and tracking using normalized cuts. In *IEEE International Conference on Computer Vision (ICCV)*, 1998. 5
- [28] H. Song, W. Wang, S. Zhao, J. Shen, and K.-M. Lam. Pyramid dilated deeper ConvLSTM for video salient object detection. In *IEEE European Conference on Computer Vision (ECCV)*. 2018. 5, 7, 8
- [29] D. Sun, J. Wulff, E. B. Sudderth, H. Pfister, and M. J. Black. A fully-connected layered model of foreground and background flow. In *IEEE Conference on Computer Vision and Pattern Recognition (CVPR)*, 2013. 5
- [30] D. Sun, X. Yang, M.-Y. Liu, and J. Kautz. Pwc-net: Cnns for optical flow using pyramid, warping, and cost volume. In *IEEE Conference on Computer Vision and Pattern Recognition (CVPR)*, 2018. 5, 6, 7

- [31] B. Taylor, V. Karasev, and S. Soatto. Causal video object segmentation from persistence of occlusions. In *2015 IEEE Conference on Computer Vision and Pattern Recognition (CVPR)*. IEEE, jun 2015. 8
- [32] P. Tokmakov, K. Alahari, and C. Schmid. Learning motion patterns in videos. In *IEEE Conference on Computer Vision and Pattern Recognition (CVPR)*, 2017. 5, 6, 7, 8
- [33] P. Tokmakov, K. Alahari, and C. Schmid. Learning video object segmentation with visual memory. In *IEEE International Conference on Computer Vision (ICCV)*, 2017. 5, 7, 8
- [34] D. Tsai, M. Flagg, and J. Rehg. Motion coherent tracking with multi-label MRF optimization. In *British Machine Vision Conference (BMVC) 2010*. British Machine Vision Association, 2010. 5, 6, 8
- [35] J. Wang and E. Adelson. Representing moving images with layers. *IEEE Transactions on Image Processing*, 3(5):625–638, 1994. 5
- [36] W. Wang, J. Shen, and F. Porikli. Saliency-aware geodesic video object segmentation. In *IEEE Conference on Computer Vision and Pattern Recognition (CVPR)*, 2015. 7
- [37] Y. Yang and S. Soatto. Conditional prior networks for optical flow. In *European Conference on Computer Vision*, pages 282–298. Springer, 2018. 5, 7
- [38] Y. Yang and G. Sundaramoorthi. Shape tracking with occlusions via coarse-to-fine region-based sobolev descent. *IEEE transactions on pattern analysis and machine intelligence*, 37(5):1053–1066, 2015. 6
- [39] Y. Yang, G. Sundaramoorthi, and S. Soatto. Self-occlusions and disocclusions in causal video object segmentation. In *Proceedings of the IEEE International Conference on Computer Vision*, pages 4408–4416, 2015. 6